HHS Public Access

Author manuscript

Nano Lett. Author manuscript; available in PMC 2018 October 11.

Published in final edited form as:

Nano Lett. 2017 October 11; 17(10): 6184–6194. doi:10.1021/acs.nanolett.7b02845.

Polypyrrole Coated Perfluorocarbon Nanoemulsions as a Sono-Photoacoustic Contrast Agent

David S. Li[1], **Soon Joon Yoon**[2], **Ivan Pelivanov**[2,3], **Martin Frenz**[4], **Matthew O'Donnell**[3], and **Lilo D. Pozzo**[1,*]

[1]Department of Chemical Engineering, University of Washington, Seattle, Washington, 98195, USA [2]Department of Bioengineering, University of Washington, Seattle, Washington, 98195, USA [3]International Laser Center, Moscow State University, Moscow, 119992, Russia [4]Institute of Applied Physics, University of Bern, Bern, CH-3012, Switzerland

Abstract

A new contrast agent for combined photoacoustic and ultrasound imaging is presented. It has a liquid perfluorocarbon (PFC) core of about 250 nm diameter coated by a 30 nm thin polypyrrole (PPy) doped polymer shell emulsion which represents a broadband absorber covering the visible and near-infrared ranges (peak optical extinction at 1050 nm). When exposed to a sufficiently high intensity optical or acoustic pulse, the droplets vaporize to form microbubbles providing a strong increase in imaging sensitivity and specificity. The threshold for contrast agent activation can further drastically be reduced by up to two orders of magnitude if simultaneously exposing them with optical and acoustic pulses. The selection of PFC core liquids with low boiling points (i.e. perfluorohexane (56°C), perfluoropentane (29°C) and perfluorobutane (−2°C)) facilitates activation and reduces the activation threshold of PPy coated emulsion contrast agents to levels well within clinical safety limits (as low as 0.2 MPa at 1 mJ/cm^2). Finally, the potential use of these nanoemulsions as a contrast agent is demonstrated in a series of phantom imaging studies.

Graphical abstract

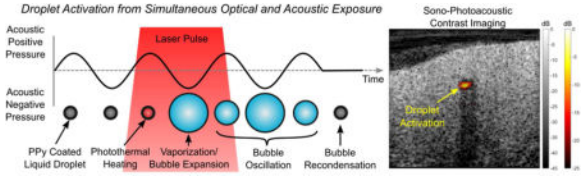

Keywords

Photoacoustics; Sono-Photoacoustics; Nanoemulsions; Bubbles; Contrast Agents; Cavitation

Contrast agents for imaging and therapy is a growing area throughout the ultrasound (US) and photoacoustic (PA) imaging communities[1–4]. In US, microbubbles are being

* dpozzo@uw.edu.

investigated for vascular imaging, drug delivery, as well as cavitation-based therapies[5–8]. Typically, microbubble size distributions are between 1–10 μm in diameter. Because of growing interest in combined therapeutic and diagnostic (i.e. theranostic) agents, there has been extensive work on reducing bubble size to the sub-micrometer range to improve agent penetration into diseased tissue and take advantage of the enhanced permeability and retention (EPR) effect. However, creating stable nanobubbles is currently a significant challenge due to their low stability[5,9–11].

In recent years, phase-change contrast agents have emerged as an alternative to microbubbles due to their longer recirculation time, stability, and relative ease of production as a nanoagent[12–14]. These nanoemulsions can be synthesized using the same low boiling point perfluorocarbon (PFC) gases as in US microbubbles, but relying on a large Laplace pressure to suppress spontaneous boiling[14,15]. As a liquid emulsion, droplets are acoustically transparent. However, if exposed to a sufficiently high intensity acoustic pulse, they undergo a phase-change producing microbubbles[16–18]. The resulting bubbles are typically over 100 times larger in volume than the initial droplets[19–22]. This approach has been coined acoustic droplet vaporization (ADV). The event itself, as well as the resulting bubbles, can be used for both imaging and therapy. Several studies have demonstrated the benefits of ADV in contrast enhancement, drug delivery, and therapy[22–25].

More recently, several phase-change PFC droplet formulations had been synthesized to incorporate optically absorbing nanoparticles or dyes for optical droplet vaporization (ODV)[26–32]. Optical absorbers associated with the droplets provide a linear photoacoustic response. However, if exposed to an optical pulse of sufficiently high-intensity, the droplets vaporize through photo-thermal heating of the associated optical absorber to generate microbubbles and non-linear PA signal enhancement providing a significantly larger PA signal than that from conventional linear PA agents, even when present at much lower concentrations[26,33]. In addition to diagnostic imaging, droplet-based PA agents have shown promising results in photo-thermal therapy and clot disruption[34,35].

Although droplet-based contrast agents are promising, the high vaporization threshold still poses a significant barrier to many PA and US applications. Several studies have confirmed that the ADV threshold can be as high as 5 MPa, while several PA droplet formulations require up to a 400 mJ/cm^2 laser fluence for activation[14,18,27,28,36–39]. In many cases, the pressures and optical fluences required to initiate droplet vaporization approach exceed FDA and ANSI limits for diagnostic purposes.

A new strategy in droplet-based contrast agents, called sono-photoacoustics (SPA), has been developed to significantly reduce the intensities needed to vaporize nanometer-sized droplets[26,33]. This technique relies on transmitting an acoustic pulse followed by a delayed laser pulse such that acoustic and optical pulses overlap in the region of interest. The combination of the acoustic negative pressure and photothermal agent heating produces a non-linear reduction in vaporization threshold compared to that for either energy source independently. The first demonstration of SPA imaging used a Pickering emulsion featuring a perfluorohexane droplet core decorated with a gold nanoparticle shell[26]. Compared to ADV and ODV thresholds, SPA thresholds were significantly reduced to 1.5 MPa at 1.24

MHz and 0.6 mJ/cm^2 at 750 nm[26]. Furthermore, SPA imaging has shown excellent contrast enhancement and specificity at picomolar agent concentrations, a level unachievable with conventional nanoparticle-based photoacoustic contrast agents[26]. In addition to diagnostic imaging, the same SPA contrast agent has demonstrated potential as a therapeutic agent for clot lysis in benchtop experiments[34]. Even though these results are promising, clinical translation will require extending the optical absorption spectra to the near-infrared (NIR) range (>800nm) to further reduce intrinsic tissue optical attenuation and potential associated damage.

In this study, we present a new type of optically and acoustically sensitive phase-change contrast agent with broad optical absorption covering both the visible and NIR ranges. They have a low boiling point liquid PFC core stabilized by an optically absorbing polypyrrole (PPy) polymer shell. Methods for agent synthesis are first presented followed by extensive physical characterization of the contrast agent. The activation threshold of the PPy coated contrast agent is measured as a function of acoustic pressure, laser fluence, and PFC core material. Finally, SPA imaging using PPy coated contrast agents is demonstrated in a tube phantom as well as in *in-vitro* chicken breast as a model of biological tissue.

The size of PPy-coated, emulsion-based contrast agents is largely dictated by the initial size of the emulsion droplets used as templates. Agent synthesis was adapted from previous methods for PPy nanoparticles as illustrated in figure 1[40,41]. Although mechanical approaches, such as high-pressure emulsification and sonication, can lead to monodisperse droplet distributions on the order of ~350 nm in diameter, the ouzo method produced droplets of significantly smaller diameter (figure 2A). Droplet size distributions from high-pressure homogenization resulted in a mean diameter of 357 nm and a polydispersity index (PDI) of 0.10. Although the droplet distribution can be further reduced through sequential homogenization steps, losses from vaporizing droplets are expected to reduce yield. Density measurements before and after homogenization revealed that as much as 90% of the PFC could be lost from unwanted vaporization. In contrast, using the ouzo approach to spontaneously nucleate droplets produced emulsions with a mean diameter of 184 nm (PDI = 0.081). No measureable PFC losses were observed in emulsions synthesized with spontaneous nucleation. Moreover, efficient production of low boiling point PFC emulsions with the ouzo approach was feasible because no mechanical forces were needed to produce these droplets, which would cause heating and unwanted PFC vaporization.

Importantly, ultraviolet-visible (UV-Vis) spectrophotometry measurements of PPy samples also show broad optical extinction covering both the visible and near-infrared (NIR) ranges. The optical extinction of the PPy-based agents was normalized according to the pyrrole monomer concentration used for synthesis. After normalizing the optical extinction, the extinction of the PPy-based agents was greater than that of gold nanoparticles on a per ion basis in the NIR range (>800nm) in figure 2B. The similarity in normalized optical extinction values between the PPy particles (no PFC core) and the unfiltered PPy coated emulsions (with PFC core) indicates that optical properties are defined by the presence of PPy. Although TEM imaging revealed that fully coated PPy PFC emulsions were formed, a significant number of solid PPy particles were also simultaneously synthesized (figure 2D). These particles are not prone to cavitation but still absorb significant fractions of the incident

light, so they should be removed to improve efficiency. Fortunately, centrifugation was found to be a straightforward approach to remove excess particles to achieve pure emulsion dispersions (See supplemental figure S1). After purification, the optical extinction of PPy-coated emulsion contrast agents was still strong across the visible and NIR ranges. The slight increase in extinction in the UV range is likely caused by increased scattering from larger emulsions. As the concentration of pyrrole was decreased (PVA and iron are also proportionally decreased), the peak optical extinction in the NIR range decreases. No observable differences in normalized UV-Vis spectra were observed between PPy emulsion samples prepared using different PFCs or between homogenized and ouzo synthesized droplets.

TEM images indicate that PPy encapsulates the PFC droplet in a core-shell structure (figure 2D). Moreover, TEM images of the emulsions suggest that the wall thickness of PPy coating the droplets is similar in size to the diameter of the solid PPy particles. Scattering profiles of the PPy particles versus PPy-coated emulsions obtained though SAXS demonstrate that the particles and emulsion share a similarly sized feature (dotted red line in figure 2C). This feature, highlighted in figure 2C, confirms that the PPy coating around the droplets is comparable in size to the diameter of a PPy particle. Model fitting of SAXS profiles was guided by results from DLS (i.e. particle diameter) and from observations made in TEM images (i.e. core-shell structure). A solid sphere model was used to fit the solid PPy particle, while a core-shell model was used to fit the PPy-coated emulsion sample scattering profiles over the q-range of 0.4 – 0.35 $Å^{-1}$[42]. The scattering length density (SLD) of the solvent (water) was fixed to 9.44×10^{-6} $Å^{-2}$ while the SLD of the polypyrrole particle was fixed to be 8.6×10^{-6} $Å^{-2}$. The fit suggests an average particle diameter of approximately 50.4 nm with an average PDI of 0.13 The particle diameters estimated from SAXS profiles files are in good agreement with previously published particle measurements[40,41].

For core-shell model fitting of the PPy-coated emulsions, the SLDs of solvent (water), PFC liquid core, and polypyrrole shell was fixed to 9.44×10^{-6} $Å^{-2}$, 12.9×10^{-6} $Å^{-2}$ and 8.6×10^{-6} $Å^{-2}$, respectively. Using the DLS measurements of the emulsions (i.e. known diameter) and the PPy particle SAXS fits as a guide, the diameter of PPy-coated emulsion core was constrained to 200 – 400 nm in diameter while the shell was constrained to 20 – 50 nm in thickness. Although particle diameter appeared to slightly decrease with decreasing PPy concentration, the diameters of the emulsion agents was nearly constant across the PPy concentrations tested. The core-shell model fits resulted in a consistent average liquid PFC inner core diameter ranging from 226 nm to 244 nm in diameter. According to the model fits, the PPy shell thickness on the droplets increased from 33.3 nm to 41.1 nm in thickness according to pyrrole concentration that was used during synthesis.

Sono-photoacoustic cavitation threshold measurements for the newly proposed PPy-coated PFC emulsions were compared to those from degassed water, solid PPy particles (i.e. no PFC core), and uncoated PPy emulsions (i.e. only PFC liquid emulsion). All measurements were conducted using the setup shown in figure 3A. The cavitation threshold for PPy particles and pure degassed water was measured to be nearly 10 MPa, with almost no dependence on laser fluence below 10 mJ/cm^2 (figure 3B).

All the PPy coated emulsion contrast agents provided much lower cavitation (activation) thresholds with a much stronger dependence on laser fluence than PPy particles alone. As expected, the activation threshold decreased as the PFC core material decreased from the highest boiling point PFC (PFH, $T_{boiling}$=56°C) to the lowest boiling point PFC (PFB, $T_{boiling}$=−2°C) (See supplemental figure S2). The specific emulsion synthesis method (i.e. ouzo or high-pressure homogenization) had no effect on activation threshold and signal intensity. Activation thresholds of uncoated PFC emulsions were measured as a control to evaluate the contribution of photo-thermal heating of the emulsion core from PPy optical absorption. Although uncoated emulsion samples provided lower cavitation thresholds than water and PPy particles, PPy-coated emulsion counterparts were far more sensitive to light (see supplemental figure S2). Importantly, the relative increase in signal generated from SPA droplet activation is considerably greater than pure water or particles alone across a majority of pressures and laser fluences (figure 3C). The signal intensity generated from PPy coated contrast agents containing PFB and PFP was also consistently greater than PPy coated contrast agents containing PFH, a perfluorocarbon of higher boiling point.

Interestingly, depending on the operating conditions, uncoated droplets with a low boiling point PFC core had a lower threshold than PPy-coated droplets with a higher boiling point perfluorocarbon. The relative importance of PFC boiling point versus the optical absorption of the PPy shell varies with operating conditions. Under the extreme scenario of nearly no optical fluence, photo-thermal heating plays little role in the vaporization threshold and an uncoated low boiling point perfluorocarbon can have a lower threshold than PPy-coated agents due to its very unstable nature (e.g. uncoated PFB versus coated PFH in supplemental figure S2A). This is caused by the increased stability that the elastic PPy shell provides. Therefore, under low light intensities the nature of the perfluorocarbon core (volatility) outweighs shell absorption properties. However, if the optical fluence increases, the relative pressure needed to initiate SPA activation reduces much more for PPy-coated droplets than for uncoated droplets. At very high laser fluences, it can be seen that even the highest boiling point PPy-coated perfluorocarbon will have a lower activation threshold than the lower boiling point (highest volatility) uncoated droplets (e.g. PPy-coated PFH versus uncoated PFB above 15 mJ/cm^2). The relative importance of optical absorption versus perfluorocarbon core volatility is therefore a non-linear mix of the two properties and will vary depending on the levels of optical fluence and acoustic pressures than are being delivered to the agents.

To validate SPA imaging using PPy-coated, emulsion-based contrast agents, four samples in thin walled plastic tubing were imaged in tandem (figure 4): cellulose, PPy particles (8.1 nM), PPy-coated PFP emulsions (0.65 pM), and water. The samples were excited with a 2-cycle acoustic pulse and irradiated at an optical fluence of 2 mJ/cm^2 in a degassed water bath at room temperature (20°C). Conventional US imaging showing the boundary of the four samples side-by-side with cellulose having the greatest US contrast because of linear acoustic scattering (figure 4). Conventional PA imaging shows a clear PA signal from the boundaries of both the PPy particles and PPy-coated PFP emulsion samples (figure 4A). Although a PA signal is generated from the entire volume of the PPy particle and PPy-coated PFP emulsion samples, the reconstructed image only shows the top and bottom boundaries due to a limited transducer aperture and limited frequency bandwidth[43,44]. The absence of

the PA signal from the cellulose and water filled tube samples confirm that the PA signal is not from light absorption within the tubing.

Above threshold, SPA imaging reveals a clear signal within the PPy-coated PFP emulsion tube sample (figure 4 B and C). Additionally, the SPA pulse sequence (eq. 1) cancels all linear PA and US signals (See supplemental figure S3). This linear cancellation of all PA and US signals removes background signals observed in conventional US and PA images. Conventional (linear) PA imaging is known to produce a signal linearly proportional to laser fluence at the light intensities used in these experiments. However, SPA imaging using PPy-coated PFP emulsions produces non-linear signal enhancement due to the phase transition of the PFC liquid core (figure 4E). By increasing the acoustic pressure during SPA imaging, an exponential increase in signal amplitude is achieved. This is highlighted in the near linear increase in SPA image contrast enhancement (slope of 35.2 dB/MPa, $R^2 = 0.94$). In contrast, conventional PA imaging provided no image contrast enhancement with increasing acoustic pressure (slope of 0.04 dB/MPa, $R^2 = 0.0009$). Moreover, at the highest acoustic pressure tested (MI=0.67, 1.16 MPa), a 22.8 dB increase in signal amplitude over conventional PA imaging was observed using SPA imaging in combination with the newly designed emulsion-based agent.

Contrast enhanced imaging from SPA droplet activation using PPy-coated PFP contrast agents was performed in a chicken breast to better mimic optical and acoustic scattering properties in clinical applications (figure 5). All experiments used a transducer and optical fiber arrangement identical to that used in the tube phantom experiment. However, the optical fluence delivered at the surface of the chicken breast was increased to 45 mJ/cm^2. The PPy-coated PFP emulsion contrast agent was contained within a thin-walled plastic tube (i.e. yellow dashed line in figure 5A) passing through the tissue. Shadowing seen in the US images is a result of acoustic reflections from the tubing.

SPA imaging of the contrast agent in tissue leads to an approximate 17.0 dB signal enhancement over conventional PA imaging under identical circumstances (figure 5). The PA image dynamic range was scaled according to the maximum SPA signal observed. SPA imaging provided a substantial improvement in specificity over PA imaging. The PA signals observed at the surface of the chicken breast (see figure 5A) were completely removed in SPA imaging (figure 5B), a direct result of linear photoacoustic signal cancellation from background subtraction built into the SPA sequence (eqn. 1). Using US imaging (MI = 0.67) and PA imaging alone, there was no perceivable signal enhancement from the contrast agent (figure 5A).

The new PPy-coated, PFP contrast agent has a broad optically absorbing shell and a low boiling point PFC liquid core. The core can be used for non-linear contrast enhancement through droplet vaporization. Furthermore, the shell provides an extinction spectrum covering the entire optical window clinically relevant to PA imaging (figure 2B), enabling PA or SPA signal over the optical tissue window range of 600–1200 nm. The possibility of using high repetition Nd:YAG lasers produced in a small and economic form factor may help rapidly translate SPA imaging into a clinical product.

Previously, the most common approach to synthesize PFB liquid nanoemulsions began by producing PFB microbubbles in water followed by a high applied pressure and a chilled ethanol bath to condense the microbubbles into nanodroplets[13,23,45]. Although the two methods presented here can create nanodroplets using highly volatile PFCs, the ouzo method is simple and eliminates the equipment required to form initial microbubbles. Conventional approaches using mechanical forces, such as sonication or high-speed shaking, to fractionate droplets often produce polydisperse distributions on the order of 1–5 micrometers in diameter[14,22]. Other mechanical approaches requiring the emulsion suspension to pass through a size controlling aperture, such as high-pressure homogenization, can easily reduce the droplet distribution to sizes as small as 357 nm and further reduce the PDI to nearly 0.1.

Here, we presented a new approach where the highly volatile PFC droplets is first dissolved in ethanol and droplets are spontaneously nucleated (ouzo method) by adding water to produce monodisperse stable droplet dispersions with a mean diameter of 184 nm (PDI = 0.08). Conventional approaches to mechanically disrupt two-phase systems to create micro-/nano-emulsions are inefficient when emulsifying highly volatile liquids such as PFB ($T_{boiling}$ = −2°C) due to unwanted vaporization. Liquid volatility poses no challenge in spontaneously nucleating nanodroplets because the system requires no mechanical forces and can be performed at either room temperature or in an ice bath. The ouzo method for emulsification requires that the solute (e.g. PFB) have very low solubility in a medium (e.g. water) and some solubility in a miscible co-solvent (e.g. ethanol). The solute, initially dissolved in the co-solvent, loses solubility as a miscible non-solvent (i.e. water) is added to the mixture. As the solubility rapidly decreases the solute forms a separate phase by spontaneously nucleating monodisperse droplets.

The size of the droplet is also known to be largely determined by the diffusion limited growth of a droplet nuclei[46]. All solutes within a well-defined finite diffusion radius are depleted during the growth of individual droplet nuclei, leading to monodisperse nanometer sized droplets[46–48]. It is also believed that 1–4 micron droplets can be produced from the ouzo method by allowing the nanodroplets to coalesce[47,48]. Coalescence and Ostwald ripening are greatly reduced by including a surfactant during the nucleation process.

The current droplet distributions are also on the edge of satisfying the size constraint for diffusing past tight junctions through the EPR effect[5,8,46]. Agents small enough to take advantage of the EPR effect could be used for extravascular diagnostic imaging and also for identifying blood clots. Furthermore, these agents have the potential for therapeutic applications where they can be violently cavitated for tumor ablation or clot lysis[5–8,12]. According to literature, if the ratio of ethanol to PFC increases in ouzo preparations, the diffusion radius should remain the same but the number of PFC molecules available to nucleate a new droplet diminishes[46]. It is possible that, by mapping out the ouzo phase diagram and further reducing the PFC concentration during ouzo synthesis, stable droplets under 100 nm could be synthesized for EPR applications[46].

PPy-coated emulsions clearly provide much lower SPA activation thresholds than either solid PPy particles or water alone. Moreover, these thresholds do not appear to depend on the core emulsion synthesis method. In the limit of pure acoustic droplet vaporization, the

thresholds for vaporization are approximately 2.3 (MI = 2.07), 3.1 (MI = 2.78), and 4.0 MPa (MI = 3.59) for PFB, PFP and PFH respectively[13,18,20,39,49]. As expected, the acoustic vaporization threshold increases with increasing PFC boiling point (decreasing volatility). No clear mechanism for droplet vaporization using a combination of light and sound has been proven to date.

It was also determined that small changes in droplet size (i.e. from 200 to 350 nm), for ouzo and ultrasound emulsification synthesis, did not produce appreciable differences in activation thresholds. Previous studies investigating the mechanism behind acoustic vaporization of perfluorocarbon drops have shown that, in large (i.e. micrometer sized) droplets, the droplet itself behaves as an acoustic lens. This lensing effect results in a droplet size dependent focal gain in acoustic pressure within perfluorocarbon microdroplets[16–18]. However, the droplet populations synthesized using high-pressure homogenization and ouzo nucleation are three orders of magnitude smaller in diameter (D_{Ouzo}=181 nm and $D_{Homogenized}$=377 nm) than an acoustic wavelength in liquid PFC (λ_{PFC} = 327 μm). These length scale discrepancies make it unlikely that acoustic focusing provides additional acoustic gain initiating ADV for these nano-sized agents.

Optical droplet vaporization (ODV) thresholds for the PPy-coated emulsions approach 11, 20, and 70 mJ/cm^2 for PB, PFP and PFH respectively. As previously discussed, the thresholds for optical vaporization increase with increasing PFC boiling point (decreasing volatility). This trend seems to agree with previously published work on ODV, concluding that photothermal heating leads to evaporation of perfluorocarbon liquid core[27,28,32,36–39]. The onset of SPA droplet vaporization, where optical fluences are below the ODV limit, is likely due to a combination of photothermal heating of the PFC core from light absorption in the PPy shell and homogenous cavitation from the acoustic rarefaction phase. This hypothesis is supported by previous studies showing that laser-illumination of optically absorbing nanoparticles during the peak-negative phase of a high-intensity ultrasound pulse can reduce the acoustic cavitation threshold.[50–52] From those studies, it was concluded that the reduction in acoustic cavitation threshold is due to local heating of the liquid surrounding the particles from photo-thermal processes. However, there was no apparent correlation between vaporization thresholds and the different size distributions resulting from the two different droplet synthesis methods. Therefore, at relative size scales where the acoustic wavelength is much longer than the droplet diameter, the similarity in vaporization threshold even with somewhat differing droplet sizes suggests that the droplets will vaporize when a combination of negative pressure and photothermal heating exceeds an intrinsic threshold for the droplet core.

The optical fluences required to activate PPy-coated droplets at the acoustic FDA limit at 1.24 MHz (MI_{Limit}=1.9, P_{Limit}=2.1 MPa) are approximately 0.02, 0.13, and 1.4 mJ/cm^2, which makes these agents ideal for deep SPA clinical imaging. Moreover, the PFH-based agent serves as a good diagnostic SPA imaging probe because the bulk boiling point of PFH is above body temperature but below water ($T_{PFH\ boiling}$ = 56°C). Because PFH has a boiling point between these limits, the droplet will recondense back into its liquid phase after activation[26,27,29,33,34]. Furthermore, because these agents can also be synthesized at diameters well less than 200 nm with the ouzo method, they should be able, when

additionally functionalized, to accumulate in tumors. The combination of small initial size and a reversible phase change makes PFH-based PPy-coated emulsions a good potential candidate for contrast-enhanced imaging of vasculature or identifying blood clots, tissue lesions, and tumors.

Even though PFP has a boiling point below body temperature ($T_{PFP\ boiling}$ = 29°C), PPy-coated PFP droplets can also be reversibly phase transitioned for repeated SPA activation events if the droplets are sufficiently small[53]. Using the ideal gas law and assuming that the increase in internal bubble pressure from the Laplace pressure dictates a stable bubble or gas to liquid condensation, we find that a critical diameter exists for PFP droplets to recondense as a function of temperature[53,54]. At body temperature, the critical diameter is 761 nm (See supplemental figure S4). If the droplet is smaller than the critical diameter, the resulting bubble after vaporization will spontaneously recondense back into its liquid phase. If the droplet is larger than the critical diameter, the resulting bubble will be stable and will not recondense. With an ouzo-based approach one can easily produce phase-reversible droplets whose diameter is well under 400 nm in diameter. Using PPy-coated PFP emulsions would provide the same functionality as the higher boiling point PFH agents. However, the higher-volatility of PFP would provide improved access to deeper tissue diagnostic imaging (~6.6 cm). PPy-coated PFP and PFH mixtures can be used to balance the stability of the higher boiling point PFH and lower SPA activation thresholds of PFP [13,23,45].

Using Laplace's law, the ideal gas law, and the phase diagram for PFB, we find that the critical diameter for PFB to reversibly recondense at body temperature is only 81 nm[54] (See supplemental figure S4). Although the highly volatile PFB-based agent ($T_{PFP\ boiling}$ = −2°C) could be used for deep tissue diagnostic imaging of tumors, soft tissue lesions, blood clots, etc. (~8.5 cm), the agent as presented is unlikely to recondense after SPA activation. Therefore, more volatile emulsions such as PFB and PFP, could be better suited for therapy applications such as HIFU ablation, blood clot erosion, sonoporation, etc[5–8,12].

In droplet-mediated SPA therapy, vaporizing all droplets in the region of interest and possibly causing internal bubble collapse may expedite tumor ablation, clot lysis, drug delivery, etc. In these applications, PPy-coated droplets can be easily synthesized under 200 nm in diameter using the ouzo method to penetrate into blood clots, extravasate into tissues with leaky vasculature, and be endocytosed into cells with appropriate functionalization of the agents for biological targeting. By vaporizing droplets after they have penetrated into a blood clot or extravasated into leaky diseased tissues, the mechanical forces from bubble expansion or inertial cavitation collapse can be leveraged for SPA mediated therapy. For clot lysis, it may be necessary to first diagnose and identify the location of the clot using a phase-reversible SPA agent such as PPy-coated PFH or PFP emulsions. This hypothesis will be tested in future studies.

In imaging studies, a finite-width plane in depth was defined by the 2-cycle plane wave transmitted by the ultrasound transducer prior to lasing. Localizing droplet activation is especially desirable in applications including cavitation-based therapeutic applications where high-amplitude bubble oscillations, and possibly inertial cavitation of the active SPA contrast agent, is desired. Further localization of agent activation can be achieved by

focusing the acoustic beam. However, in some cases a larger imaging plane is required, such as identifying the location of the contrast agent. In these scenarios, a combination of longer acoustic pulses and sweeping laser delays to capture multiple SPA images at different depths can be used to satisfy larger SPA imaging field requirements. Conversely, once a region of interest is identified, a fixed laser time delay and acoustic pulse duration can be used to localize agent excitation and maximize frame rate.

The SPA imaging sequence requires four US shots (2 pulse inversion pairs) and two laser shots. In this study, SPA images were collected, processed, and displayed in real time at 10 Hz and interleaved with conventional US images. The factor limiting the frame rate was the maximum laser pulse repetition rate of 20 Hz. We anticipate that the SPA frame rate can be easily increased to hundreds of hertz and more using faster pulse rate lasers delivering light at wavelengths near 1064 nm where highly efficient, compact, and cost-effective diode-pumped devices are available.

Under identical imaging conditions, a single SPA contrast image using the PPy-coated emulsion contrast agent provided an increase in image contrast of 23 dB over single shot conventional PA imaging (H_{sample}=2 mJ/cm^2). Moreover, contrast enhancement using SPA imaging in combination with the PPy-coated emulsion contrast agents was also obtained using an agent concentration of 0.65 pM versus 8.1 nM of particles for conventional PA imaging. To the best of our knowledge, picomolar sensitivity is currently unattainable using conventional particles and PA imaging techniques. Furthermore, the SPA imaging conditions tested used plane waves at a MI below 0.67, well under FDA diagnostic limits of 1.9.

The non-linear SPA signal detected is from droplet vaporization and bubble oscillation. Below the SPA activation (or cavitation) threshold, the agent behaves like a conventional dye or particle based linear PA agent producing a thermo-elastic pressure wave. According to the literature, in the dilute regime where droplet-droplet interactions can be neglected, the vaporization threshold of droplets should be independent of concentration and pulse duration[20,39,55]. Although the threshold for activation may be concentration independent, the signal amplitude from the activated agents should increase linearly with increasing concentration.

In conclusion, we presented a new phase-change contrast agent designed for SPA imaging. It features an optically absorbing PPy polymer shell, enabling agent activation using 1064 nm wavelength lasers for improved optical depth of penetration. Furthermore, these agents feature a low-boiling point PFC core, providing threshold-based, non-linear signal enhancement droplet vaporization. Finally, all components in these emulsion-based contrast agents are FDA approved in other applications. We anticipate that they should have improved biocompatibility relative to other PA contrast agents using metallic nanoparticles. Although these contrast agents can be used for conventional US or PA imaging, the dramatic enhancement is achieved at much lower pressures and laser fluences using simultaneous activation through SPA imaging. Our experiments revealed that these agents offer high spatial selectivity with signal amplitudes similar to microbubbles in US images through droplet vaporization while providing the molecular specificity of PA imaging. Because of non-linear signal enhancement from droplet vaporization, they produce contrast

enhancement orders of magnitude greater than conventional PA imaging agents at centimeter depths and picomolar concentrations (0.65 pM) in phantom studies. Due to the low optical fluence needed for activation, we expect that they can be used at depths up to several centimeters into tissue. Finally, because of their small size, these novel agents can also prove attractive for combined diagnostic imaging and targeted or localized US/PA therapies.

Experimental Section

NANOPARTICLE SYNTHESIS

Polypyrrole (PPy) nanoparticles were synthesized using a method adapted from Hong, et al. 2010[40,41]. In brief, a stock solution of 31 kDa polyvinyl alcohol (PVA) (CAS: 9002-89-5, Sigma-Aldrich, St. Louis, MO, USA) was dissolved into deionized (DI) water at 8% by weight and filtered through a 0.45 μm filter. The PVA solution was then transferred by pipette into a glass vial and diluted with DI water to the desired molar quantity. A 0.8 M stock solution of aqueous iron (III) chloride (CAS: 7705-08-0, Sigma-Aldrich, St. Louis, MO, USA) solution was prepared, filtered, and added to the PVA solution. The solution was mixed for half an hour at 4°C allowing formation of iron-PVA complexes. Finally, pyrrole monomer (CAS: 203-714-7, Sigma-Aldrich, St. Louis, MO, USA) was added to the iron-PVA solution. The solution was stirred at 4°C for a minimum of 24 hours before further characterization. In all samples, the ratio of pyrrole monomer to iron was fixed (1:2 molar concentration) as well as iron ions to PVA polymer chains (200:1 molar concentration). The pyrrole concentration in the final solution was also varied from 4 mM to 43 mM.

EMULSION SYNTHESIS

Three PFCs were used for emulsion synthesis: perfluorobutane (PFB, C_4F_{10}, $T_{Boiling}$ = −2°C) (CAS: 355-25-9, Fluoromed, Round Rock, TX, USA), perfluoropentane (PFP, C_5F_{12}, $T_{Boiling}$ = 29°C) (CAS: 678-26-2, SynQuest Laboratories, Alchua, FL, USA), and perfluorohexane (PFH, C_6F_{14}, $T_{Boiling}$ = 56°C) (CAS: 355-42-0, SynQuest Laboratories, Alchua, FL, USA). Emulsification with mechanical (high-pressure emulsification) and chemical (spontaneous emulsification) routes was explored to synthesize agents. High-pressure homogenization could only be performed with PFCs having boiling points above room temperature to limit inadvertent vaporization (i.e. PFP and PFH). In contrast, spontaneous nucleation of oil droplets (i.e. ouzo method) could be successfully utilized to emulsify all PFCs, including those that are gas at ambient conditions (e.g. PFB). This new approach takes advantage of the very low solubility of PFCs in water and their partial solubility in ethanol and other alcohols. By initially dissolving PFCs in ethanol followed by the addition of water, the solubility of the PFC rapidly decreases in the ethanol-water mixture. As a result, PFC is thermodynamically forced out of solution leading to the spontaneous formation of nanometer-sized droplets. This approach has been used for centuries to create alcoholic drinks from liquors containing anise oil, such as ouzo (from Greece) and pastis (from France), that readily phase-separate into a milky solution upon mixing with water. In previous studies, the physicochemical mechanism has been described in detail and has also been used for the synthesis of micro-/nano-droplets as well as nanoparticles[46–48,56].

For PFP and PFH ouzo emulsions, PFC liquids were directly transferred by pipette into the ethanol at 2.5% by volume (measured gravimetrically). The PFC solution in ethanol was agitated until the PFC was completely dissolved. For PFB, gas was bubbled into a sealed vessel at 1 PSI containing ethanol chilled by an ice bath. The headspace in the vessel was purged three times before the valve to the vessel was closed and PFB was bubbled through the ethanol for 2 minutes to saturate the ethanol with the PFB. The PFC-ethanol mixture was then added to the PVA solution before the addition of iron (III) chloride and pyrrole to complete the PPy emulsion synthesis. The addition of water to the PFC-ethanol mixture immediately nucleated a nanoemulsion stabilized by dissolved PVA.

To create PFC emulsion stock dispersion using high-pressure homogenization, PFC liquid was transferred into water at 3% by volume (measured gravimetrically). A coarse emulsion was first formed through 20 seconds of sonication (1 second on, 1 second off, 10 seconds of total sonication time) (Digital Sonifier 450, Branson, Danbury, CT, USA) in an ice bath at 30% amplitude. The emulsion was then passed through the high-pressure homogenizer (EmulsiFlex-B15, Avestin, Ottawa, Ontario, Canada) at 24,000 PSI to create a relatively monodisperse perfluorocarbon emulsion (average diameter of approximately 250 nm with a PDI of 0.15).

PPY-COATED CONTRAST AGENT SYNTHESIS

PPy-coated PFC emulsions were synthesized in a similar manner to PPy nanoparticles (figure 1). A stock solution of 31 kDa PVA was first dissolved in DI water at 8% by weight and filtered to form a PVA stock solution. The PVA solution was then transferred by pipette into a glass vial and diluted using water for the desired final PVA quantity and concentration. In a separate container, PFC emulsion stock was prepared through one of two methods: high-pressure homogenization or spontaneous nucleation (ouzo method)[47,48]. The emulsion stock was then transferred by pipette into the PVA solution and stirred for 15 minutes at 4°C.

A 0.8 M stock solution of iron (III) chloride in water was then prepared, filtered, and added to the PVA-emulsion solution. The iron-PVA-emulsion mixture was stirred for 30 minutes at 4°C to allow iron-PVA complexation to occur along the droplet oil-water interface before the pyrrole monomer was added. After the addition of pyrrole, the solutions were mixed at 4°C for a minimum of 24 hours to complete polymerization before testing and characterization.

The emulsions were centrifuged at 1000 G for 20 min to separate PPy-coated emulsions from excess PPy particles (i.e. those with no PFC core) that may have also formed and also remove any remaining ethanol from the ouzo emulsion synthesis. The liquid supernatant was decanted and the concentrated precipitate (pellet), which contained the emulsion agents, was resuspended in pure DI water. Centrifugation and resuspension was repeated three times. The final PFC concentration in solution during synthesis was fixed at 0.75% volume. The molar ratios of iron-to-PVA (200:1 molar concentration) and iron-to-pyrrole (2:1 molar concentration) were fixed. For this study, the total concentration of pyrrole added to the final solution was varied from 4 mM to 43 mM.

OPTICAL AND STRUCTURAL CHARACTERIZATION

Optical extinction spectra for all samples were measured using ultraviolet-visible (UV-Vis) light spectrophotometry (Thermo Scientific Evolution 300, Thermo-Fisher Scientific Inc., Waltham, MA, USA) over the wavelength range of 300 – 1100 nm. The size distribution of the samples was measured through dynamic light scattering (DLS) using a Malvern Zetasizer Nano ZS, (Malvern Instruments Ltd., Worcestershire, United Kingdom). The structure of lyophilized samples was examined using transmission electron microscopy (TEM) (Tecnai G2 F20, FEI Hillsboro, OR, USA) operated at 200kV.

A more detailed structural analysis of samples was achieved using small-angle X-ray scattering (SAXS) on the 12-ID-B beamline at the Advanced Photon Source (Argonne National Lab, Argonne, IL, USA) over a Q-range of 0.002 to 0.1 $Å^{-1}$ in a pinhole configuration. The samples for SAXS measurements were dispersed in aqueous solutions held in 1.5 mm diameter quartz capillary tubes (Hampton Research, Aliso Viejo, CA, USA). Scattering profiles of the samples were normalized using water background subtraction and data were fit using the SASView package (SASView, http://www.sasview.org) to extract additional structural information. PPy particles (no PFC core) were fit using a sphere model while the emulsions (PPy coated PFC emulsions) were fit using a core-shell model[42]. The particle size and scattering length densities (SLD) of the samples were constrained during fitting using known compositions and the particle diameters from DLS measurements and TEM. Known benefits of SAXS measurements are that structural parameters are averaged over many particles within the illuminated volume and that samples do not need to be treated in any special way. In contrast, other methods risk alterations to the structure from sample preparation protocols (e.g. dehydration for TEM imaging) or limit the analysis to a small number of visualized particles.

MEASUREMENT OF CAVITATION THRESHOLDS

The cavitation setup and processing method is described in detail in Arnal et al. 2015[26]. Quantitative cavitation threshold measurements were performed using a custom made thin-walled plastic sample holder. The sample was positioned in the center of overlapping acoustic (−6 dB profile of 13.3 mm long and 1.6 mm wide) and optical fields (1/e beam width of 3.9 mm) positioned orthogonal to each other (see figure 3A). A 10 cycle long acoustic pulse was generated from a spherically focused ultrasound transducer (H-102, Sonic Concept, Woodinville, WA, USA, focus at 63 mm, f-number = 0.98, 1.24 MHz) in line with a 55 dB gain linear RF amplifier (ENI-A150, Electronics & Innovation Ltd., Rochester, NY, USA). A 5 ns long 1064 nm laser pulse was generated from a Nd:YAG laser source (Surelite, Continuum, Santa Clara, CA, USA). The laser pulse was delayed by 44 microseconds relative to the ultrasound pulse to ensure that the optical pulse coincided with the 4^{th} rarefactional acoustic cycle at the focus. The laser intensity was adjusted using a combination of neutral density (ND) filters and remotely changed using a 6 position electronically controlled filter wheel (FW-103, Thorlabs, NJ, USA). The transmitted acoustic pressure was varied from 0 MPa to 7.2 MPa, while transmitted laser pulses were varied from 0 to 88 mJ/cm^2 at the sample.

The ultrasound transducer was calibrated using a fiber optic hydrophone (FOPH 2000, RPI Acoustics, Germany). The laser pulse energy was calibrated using an energy meter (Nova II, Ophir, North Logan, UT, USA). The optical beam profile of the laser was determined by measuring the photoacoustic signal intensity of a 0.3 mm graphite target scanned in water.

Cavitation noise was detected using an in-house designed, unfocused, 28 μm thick, ultra-wideband polyvinylidene difluoride (PVDF) transducer operated in an open-circuit regime positioned beneath the sample holder (35 mm away). The transducer bandwidth approaches 40 MHz with nearly constant sensitivity (11.3 μV/Pa). The PVDF transducer used for passive cavitation detection was connected to a preamplifier (Precision Acoustics, Dorchester, UK) and signals were digitized and recorded using a Gage card (Razor 14, Dynamic Systems LLC, Lockport, IL, USA). 200 signals collected at 20 Hz were recorded for every given combination of acoustic pressure and laser optical fluence.

CAVITATION DATA PROCESSING

The cavitation signal was isolated by subtracting an averaged background signal containing the linear photoacoustic and acoustic signals. A 10 μs time window centered on the triggering of the laser shot was used to compare the average integrated cavitation signal intensity from the background noise level. Events with an integrated intensity nine times greater than time-averaged background integrated intensity were registered as cavitation events. The process was repeated for each combination of acoustic pressure and laser fluence. A sigmoid curve was fit to the cavitation probability values for a given laser fluence as a function of increasing pressure. The cavitation threshold was then defined as the 50% cavitation probability along the sigmoid fit[26].

SAMPLE PREPARATION FOR SONO-PHOTOACOUSTIC TESTING

All samples were diluted with degassed water prior to cavitation (activation) measurements. All emulsion containing samples were diluted to an estimated concentration ranging from 3.9×10^8 to 6.2×10^8 droplets/ml (0.65 pM to 1.03 pM). The PPy particle samples were diluted to an estimated concentration of 4.9×10^{12} particles/ml (8.1 nM). At these sample concentrations, it was determined that there was no thermal and acoustic coupling between fields from individual droplets. Thus, measured thresholds were considered as thresholds inherent to isolated single droplets and, therefore, will not change with further dilution of the solution.

Previous studies using nanoemulsions have concluded that low boiling point droplet activation can reversibly recondense back into its liquid phase due to the high Laplace pressure. Our initial studies confirmed that our droplets could be repeatedly activated using SPA activation. However, SPA signal intensity from droplet activation linearly decayed to half max after approximately 12 thousand activation events. For threshold measurements, the samples were exposed to a maximum of six thousand optical and/or acoustic exposures before flushing the sample holder with degassed water, refilling the sample holder with fresh sample, and continuing the SPA threshold measurements (See supplemental figure S5). Flushing and refilling the sample holder helped minimize inconsistencies in signal intensity due to droplet destruction. A static sample with periodic flushing and refilling was selected

over continuous perfusion of the sample to minimize possible motion artifacts that could confound measurements.

SONO-PHOTOACOUSTIC IMAGING

To mimic a clinical situation, a linear array transducer (ATL L7-4, 128 elements, Philips, Bothell, WA, USA) controlled by a programmable ultrasound scanner (Vantage 128, Verasonics, Redmond, WA, USA) was used both to excite the contrast agent and detect relevant US signals. The following custom SPA imaging pulse sequence was applied:

$$\mathrm{SPA} = \left\{ \mathrm{PAUS}^{+} - US^{+} \right\} - \left\{ \mathrm{PAUS}^{-} - US^{-} \right\} \quad (1)$$

where *PAUS* denotes simultaneous plane wave acoustic and laser firing and *US* indicates plane wave acoustic pulses. The +/− superscripts represent positive or negative phase first in the transmitted acoustic pulse. The $PAUS^{+/-} - US^{+/-}$ halves of the SPA sequence are used to remove linear US signal sources such as those from native tissue. Subtraction of the two terms in brackets in Eq. (1) removes linear photoacoustic signals generated from sources such as endogenous chromophores (see supplemental figure S3). Conventional US images used in the SPA image overlays were interleaved with SPA image acquisitions. The methodology behind the SPA pulse sequence is described in detail in Arnal, et al. 2015[33].

The laser emission generated at 1064 nm by a Nd:YAG laser source was delivered through a custom made bifurcating fiber optic bundle (Fiberoptic, Switzerland). Each bifurcation from the fiber bundle produced a diverging 1 mm × 15 mm (NA = 0.2) beam that was oriented on axis to the direction of acoustic propagation from the linear ultrasound array (figure 4D). Again, the timing of the Nd:YAG laser was programmed such that both the optical and acoustical pulse coincide at the focus position.

SONO-PHOTOACOUSTIC TUBE PHANTOM IMAGING CONDITIONS

SPA imaging using the newly formulated agents were compared with images from two other samples held within 4 mm transparent tubes (wall thickness of 150 μm) (figure 4) using the transducer and fiber bundle configuration shown in figure 4D. The samples imaged contained cellulose, PPy particles (i.e. no PFC core), PPy-coated PFP emulsion, and a water filled tube. The four samples were selected to compare an ultrasound scatterer (cellulose) and linear photoacoustic agent (PPy particle) against the non-linear SPA contrast agent (i.e. PPy-coated PFP emulsion). The water-filled tube was used as a control to confirm that photoacoustic and SPA signals were not generated solely from the tube wall. The emulsion sample was diluted to a concentration of 3.9×10^{8} droplets/ml (0.65 pM) while the particle sample was diluted to 4.9×10^{12} particles/ml (8.1 nM) before imaging.

SPA images were collected using a 3 MHz 2-cycle US burst excitation with a mechanical index (MI) as high as 0.67 ($P_{Negative}$ = 1.16) and a laser fluence of 2 mJ/cm^2 on the samples. The four samples were positioned side by side, approximately 1 mm between each sample, 18 to 20 mm away from the transducer. They were submerged in a degassed water bath held at room temperature (25°C).

SONO-PHOTOACOUSTIC (SPA) CHICKEN BREAST IMAGING CONDITIONS

SPA imaging, using the transducer and fiber bundle configuration shown in figure 4D, was performed on chicken breast to validate that the same SPA imaging methodology would apply to highly scattering tissue. Fresh, unfrozen chicken breast was acquired from a local butcher. The chicken was cleaned and degassed in DI water for imaging. A 4 mm thin-walled plastic tube containing the PPy-coated PFP emulsion contrast agent was passed through the tissue. Images were acquired using the same transducer and optical fiber bundle configuration as the SPA tubing phantom imaging experiments. However, the optical fluence on the surface of the chicken was increased to 45 mJ/cm^2, over a factor of two below the maximum permissible skin exposure limits for 1064 nm wavelength lasers.

Supplementary Material

Refer to Web version on PubMed Central for supplementary material.

Acknowledgments

The research performed was primarily supported by the National Institutes of Health under grant R01HL125339. Additional support was provided by National Institutes of Health grants R01EB016034, R01CA170734, R01EB009682, R01HL093140, R01DC010201, and R01EY026532 as well as the Life Sciences Discovery Fund 3292512 and Swiss-TransMed platform “ONIRIUS”. The TEM imaging work was conducted at the Molecular Analysis Facility, a National Nanotechnology Coordinated Infrastructure site at the University of Washington, supported in part by the National Science Foundation (grant ECC-1542101), the University of Washington, the Molecular Engineering & Sciences Institute, the Clean Energy Institute, and the National Institutes of Health. The SAXS measurements used resources of the Advanced Photon Source, a U.S. Department of Energy (DOE) Office of Science User Facility operated for the DOE Office of Science by Argonne National Laboratory under Contract No. DE-AC02-06CH11357. This work benefitted from SasView software, originally developed by the DANSE project under NSF award DMR-0520547. Finally, we would also like to thank FiberOptic in Switzerland for their generous donation of the custom-made fiber optic bundle used to couple the 1064 nm laser for the SPA and PA images presented.

References

1. Agarwal A, Huang SW, O’Donnell M, Day KC, Day M, Kotov N, Ashkenazi SJ. Appl Phys. 2007; 102(6):64701.
2. Chen Y-S, Frey W, Kim S, Kruizinga P, Homan K, Emelianov S. Nano Lett. 2011; 11(2):348–354. [PubMed: 21244082]
3. Li P-C, Wei C-W, Liao C-K, Chen C-D, Pao K-C, Wang C-RC, Wu Y-N, Shieh D-B. IEEE Trans Ultrason Ferroelectr Freq Control. 2007; 54(8):1642–1647. [PubMed: 17703668]
4. Kim K, Huang S-W, Ashkenazi S, O’Donnell M, Agarwal A, Kotov NA, Denny MF, Kaplan MJ. Appl Phys Lett. 2007; 90(22):223901.
5. Cavalli R, Bisazza A, Trotta M, Argenziano M, Civra A, Donalisio M, Lembo D. Int J Nanomedicine. 2012; 7:3309–3318. [PubMed: 22802689]
6. Ferrara K, Pollard R, Borden M. Annu Rev Biomed Eng. 2007; 9(1):415–447. [PubMed: 17651012]
7. Unger EC, Porter T, Culp W, Labell R, Matsunaga T, Zutshi R. Adv Drug Deliv Rev. 2004; 56(9): 1291–1314. [PubMed: 15109770]
8. Wei K, Jayaweera AR, Firoozan S, Linka A, Skyba DM, Kaul S. Circulation. 1998; 97(5):473–483. [PubMed: 9490243]
9. Gao Y, Hernandez C, Yuan H-X, Lilly J, Kota P, Zhou H, Wu H, Exner AA. Nanomedicine. 2017; 13(7):2159–2168. [PubMed: 28603079]
10. Perera RH, Wu H, Peiris P, Hernandez C, Burke A, Zhang H, Exner AA. Nanomedicine. 2017; 13(1):59–67. [PubMed: 27565686]

11. Wu H, Rognin NG, Krupka TM, Solorio L, Yoshiara H, Guenette G, Sanders C, Kamiyama N, Exner AA. Ultrasound Med Biol. 2013; 39(11):2137–2146. [PubMed: 23932272]
12. Rapoport N, Nam K-H, Gupta R, Gao Z, Mohan P, Payne A, Todd N, Liu X, Kim T, Shea J, Scaife C, Parker DL, Jeong E-K, Kennedy AM. J Control Release. 2011; 153(1):4–15. [PubMed: 21277919]
13. Sheeran PS, Wong VP, Luois S, McFarland RJ, Ross WD, Feingold S, Matsunaga TO, Dayton PA. Ultrasound Med Biol. 2011; 37(9):1518–1530. [PubMed: 21775049]
14. Kripfgans OD, Fabiilli ML, Carson PL, Fowlkes JB. J Acoust Soc Am. 2004; 116(1):272–281. [PubMed: 15295987]
15. Mountford PA, Borden MA. Adv Colloid Interface Sci. 2016; 237:15–27. [PubMed: 27574721]
16. Li DS, Kripfgans OD, Fabiilli ML, Brian Fowlkes J, Bull JL. Appl Phys Lett. 2014; 104(6):63703.
17. Shpak O, Verweij M, Vos HJ, de Jong N, Lohse D, Versluis M. Proc Natl Acad Sci USA. 2014; 111(5):1697–1702. [PubMed: 24449879]
18. Miles CJ, Doering CR, Kripfgans OD. J Appl Phys. 2016; 120(3):34903.
19. Wong ZZ, Kripfgans OD, Qamar A, Fowlkes JB, Bull JL. Soft Matter. 2011; 7(8):4009.
20. Kripfgans OD, Fowlkes JB, Miller DL, Eldevik OP, Carson PL. Ultrasound Med Biol. 2000; 26(7): 1177–1189. [PubMed: 11053753]
21. Qamar A, Wong ZZ, Fowlkes JB, Bull JL. Appl Phys Lett. 2010; 96(14):143702. [PubMed: 20448802]
22. Samuel S, Duprey A, Fabiilli ML, Bull JL, Fowlkes JB. Microcirculation. 2012; 19(6):501–509. [PubMed: 22404846]
23. Sheeran PS, Luois SH, Mullin LB, Matsunaga TO, Dayton PA. Biomaterials. 2012; 33(11):3262–3269. [PubMed: 22289265]
24. Fabiilli ML, Lee JA, Kripfgans OD, Carson PL, Fowlkes JB. Pharm Res. 2010; 27(12):2753–2765. [PubMed: 20872050]
25. Zhang M, Fabiilli ML, Haworth KJ, Fowlkes JB, Kripfgans OD, Roberts WW, Ives KA, Carson PL. Ultrasound Med Biol. 2010; 36(10):1691–1703. [PubMed: 20800939]
26. Arnal B, Perez C, Wei C-W, Xia J, Lombardo M, Pelivanov I, Matula TJ, Pozzo LD, O'Donnell M. Photoacoustics. 2015; 3(1):3–10. [PubMed: 25893169]
27. Hannah AS, VanderLaan D, Chen Y-S, Emelianov SY. Biomed Opt Express. 2014; 5(9):3042. [PubMed: 25401018]
28. Strohm E, Rui M, Gorelikov I, Matsuura N, Kolios M. Biomed Opt Express. 2011; 2(6):1432. [PubMed: 21698007]
29. Luke GP, Hannah AS, Emelianov SY. Nano Lett. 2016; 16(4):2556–2559. [PubMed: 27035761]
30. Fernandes DA, Fernandes DD, Li Y, Wang Y, Zhang Z, Rousseau D, Gradinaru CC, Kolios MC. Langmuir. 2016; 32(42):10870–10880.
31. Chen Y-S, Yoon SJ, Frey W, Dockery M, Emelianov S. Nat Commun. 2017; 8:15782. [PubMed: 28593942]
32. Yu J, Chen X, Villanueva FS, Kim K. Appl Phys Lett. 2016; 109(24):243701.
33. Arnal B, Wei C-W, Perez C, Nguyen T-M, Lombardo M, Pelivanov I, Pozzo LD, O'Donnell M. Photoacoustics. 2015; 3(1):11–19. [PubMed: 25893170]
34. Wei C, Xia J, Lombardo M, Perez C, Arnal B, Larson-Smith K, Pelivanov I, Matula T, Pozzo L, O'Donnell M. Opt Lett. 2014; 39(9):2599–2602. [PubMed: 24784055]
35. Liu W-W, Liu S-W, Liou Y-R, Wu Y-H, Yang Y-C, Wang C-RC, Li P-C. Sci Rep. 2016; 6:24753. [PubMed: 27094209]
36. Dove JD, Mountford PA, Murray TW, Borden MA. Biomed Opt Express. 2014; 5(12):4417. [PubMed: 25574448]
37. Wilson K, Homan K, Emelianov S. Nat Commun. 2012; 3:618. [PubMed: 22233628]
38. Wei C, Lombardo M, Larson-Smith K, Pelivanov I, Perez C, Xia J, Matula T, Pozzo D, O'Donnell M. Appl Phys Lett. 2014; 104(3):33701.
39. Lo AH, Kripfgans OD, Carson PL, Rothman ED, Fowlkes JB. IEEE Trans Ultrason Ferroelectr Freq Control. 2007; 54(5):933–946. [PubMed: 17523558]

40. Hong J-Y, Yoon H, Jang J. Small. 2010; 6(5):679–686. [PubMed: 20127667]
41. Zha Z, Deng Z, Li Y, Li C, Wang J, Wang S, Qu E, Dai Z. Nanoscale. 2013; 5(10):4462–4467. [PubMed: 23584573]
42. Guinier, A., Fournet, G. Small-angle scattering of X-rays. John Wiley and Sons, Inc; New York: 1955.
43. Khokhlova, T., Pelivanov, I., Karabutov, A. In Handbook of Photonics for Biomedical Science. Tuchin, V., editor. Vol. 20102371. CRC Press; 2010. p. 343-360.Series in Medical Physics and Biomedical Engineering
44. Zhang C, Chen S, Ling T, Guo LJ. J Light Technol. 2015; 33(20):4318–4328.
45. Matsunaga TO, Sheeran PS, Luois S, Streeter JE, Mullin LB, Banerjee B, Dayton PA. Theranostics. 2012; 2(12):1185–1198. [PubMed: 23382775]
46. Lepeltier E, Bourgaux C, Couvreur P. Adv Drug Deliv Rev. 2014; 71:86–97. [PubMed: 24384372]
47. Vitale SA, Katz JL. Langmuir. 2003; 19(10):4105–4110.
48. François G, Katz JL. Chemphyschem. 2005; 6(2):209–216. [PubMed: 15751338]
49. Giesecke T, Hynynen K. Ultrasound Med Biol. 2003; 29(9):1359–1365. [PubMed: 14553814]
50. Farny CH, Wu T, Holt RG, Murray TW, Roy RA. Acoust Res Lett Online. 2005; 6(3):138–143.
51. Ju H, Roy RA, Murray TW. Biomed Opt Express. 2013; 4(1):66. [PubMed: 23304648]
52. McLaughlan JR, Roy RA, Ju H, Murray TW. Opt Lett. 2010; 35(13):2127–2129. [PubMed: 20596168]
53. Asami, R., Kawabata, K. In 2012 IEEE International Ultrasonics Symposium; IEEE; 2012. p. 1200-1203.
54. Lemon, EW., McLinden, MO., Friend, DG. Thermophysical Properties of Fluid Systems. Linstrom, PJ., Mallard, WG., editors. National Institute of Standards and Technology; Gaithersburg, MD:
55. Fabiilli ML, Haworth KJ, Fakhri NH, Kripfgans OD, Carson PL, Fowlkes JB. IEEE Trans Ultrason Ferroelectr Freq Control. 2009; 56(5):1006–1017. [PubMed: 19473917]
56. Kotta S, Khan AW, Pramod K, Ansari SH, Sharma RK, Ali J. Expert Opin Drug Deliv. 2012; 9(5): 585–598. [PubMed: 22512597]

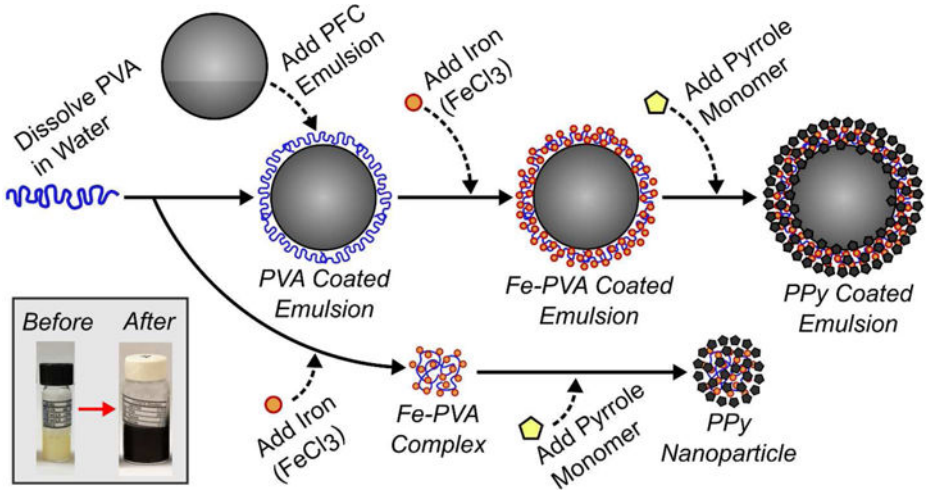

Figure 1.

Flow chart illustrating the method to synthesize polypyrrole (PPy) particles (lower pathway) and PPy coated emulsions (upper pathway). Polyvinyl alcohol (PVA) is added to a perfluorocarbon (PFC) emulsion and it adsorbs at the oil-water interface leading to stabilization. The subsequent addition of iron (III) chloride to the solution leads to the formation of iron-PVA complexes at the oil-water interface. Upon addition of pyrrole monomer, the iron (III) ions cause the localized oxidative polymerization of polypyrrole (PPy) and the formation of a core-shell PFC emulsion agent. In a simultaneous process (lower pathway), oxidative polymerization of PPy can also occur when there is an excess of iron-PVA complexes in solution leading to the formation of solid PPy particles (i.e. no PFC core). Emulsions are easily isolated from excess PPy particles through centrifugation. The insert figure (lower left) shows emulsion samples before and after polymerization of the PPy coating. The method for producing PPy coated emulsions was adapted from previous ones to produce PPy nanoparticles[40,41]. Any method producing a PFC liquid emulsion (e.g. sonication, homogenization, and spontaneous nucleation) can be used to create SPA agents.

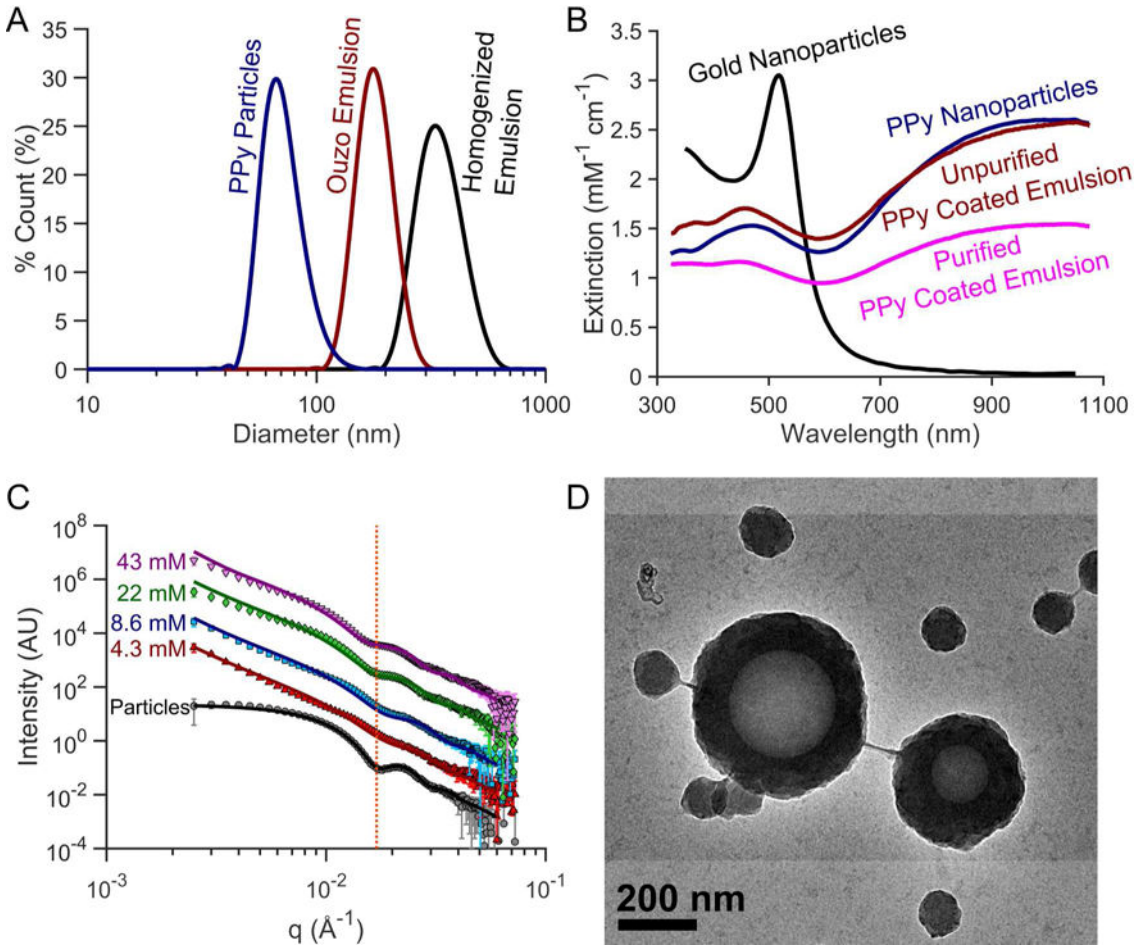

Figure 2.

(A) Dynamic light scattering (DLS) particle size distribution, (B) optical extinction spectra, (C) small-angle X-ray scattering (SAXS), and (D) transmission electron microscopy (TEM) image of PPy-coated contrast agents. (A) PPy coated emulsion contrast agents synthesized using high-pressure homogenization produce nanoemulsions between 300–400 nm in diameter. Spontaneously nucleating the droplets for PPy coated emulsion contrast agents can easily produce smaller, monodisperse droplets. The homogenized droplets shown are 357 nm (Polydispersity index (PDI) = 0.102) while the ouzo synthesized droplets were 184 nm (PDI = 0.081) in diameter. (B) PPy-based contrast agents exhibit optical extinction per particle comparable to gold nanoparticles with the added benefit of a broader optical extinction spectrum in the near IR covering the optical diagnostic window for in vivo photoacoustic imaging. (C) SAXS profiles show similar scattering patterns between PPy coated emulsions synthesized with varying pyrrole concentrations, which are also distinctly different from the scattering from solid PPy particles. The line shown in panel C highlights the inflection corresponding to the shell thickness of PPy-coated emulsions. From SAXS data fitting, as the pyrrole concentration reduces from 43mM to 4.3mM, the shell thickness decreases from 41.1 nm to 33.3 nm. SAXS profiles of the particle sample were shifted down two decades while the 8.6, 22, and 43 mM profiles were shifted 1, 2, and 3 decades above the 4.3 mM curve for ease of visualization. The emulsions were isolated from excess

particles by centrifuging, removing the supernatant containing the excess particles and resuspending the sedimented emulsion in filtered DI water.

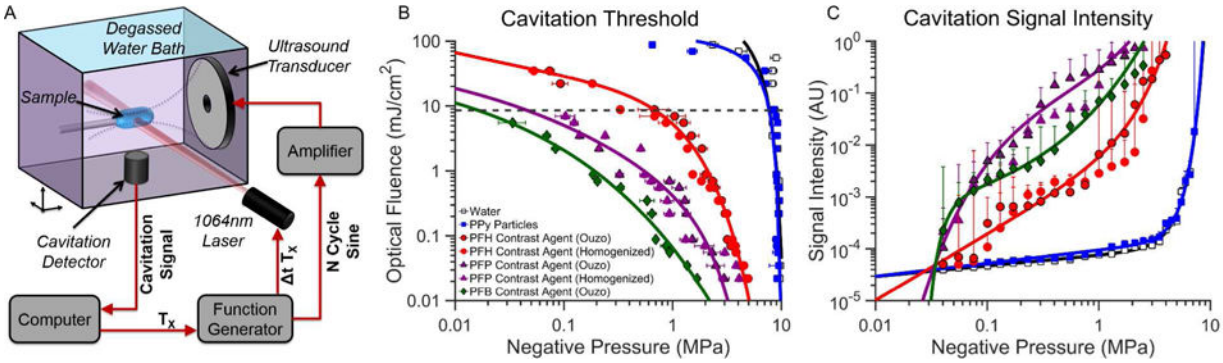

Figure 3.

(A) Schematic of the setup used for sono-photoacoustic (SPA) cavitation threshold measurements. (B) Cavitation threshold of PPy-coated emulsion contrast agents. (C) Average cavitation signal intensity as a function of negative pressure for a laser fluence of 9 mJ/cm^2. Cavitation events were initiated using a 1064 nm pulsed laser and a 1.24 MHz spherically focused ultrasound transducer. Cavitation of the PPy emulsion contrast agents creates transiently oscillating perfluorocarbon bubbles that can be used for contrast-enhanced imaging or therapy. The cavitation (or activation) threshold for the PPy emulsion contrast agents is significantly lower than water or PPy particles (no PFC core). The cavitation threshold for PPy emulsions decreases as lower boiling point PFCs are used as the core material. No significant differences in cavitation threshold and intensity were observed using PPy emulsions of the same PFC core but different emulsification methods (i.e. homogenization versus ouzo nucleation).

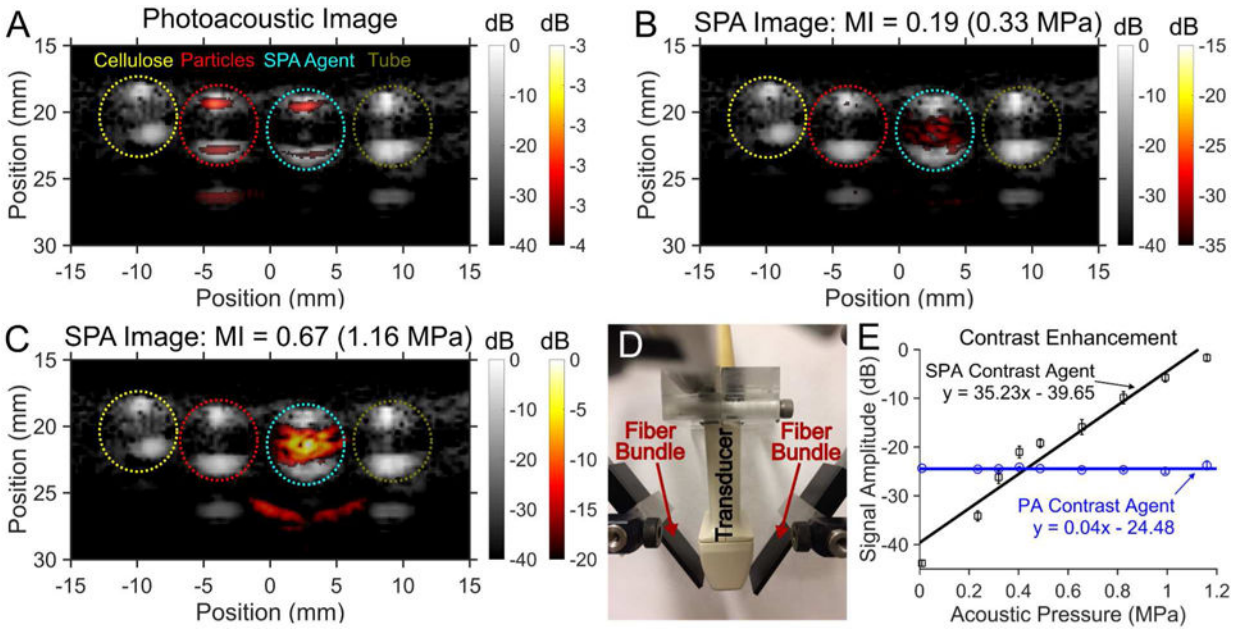

Figure 4.

The image panels compare the images and contrast enhancement from (A) photoacoustic (PA) imaging and sono-photoacoustic (SPA) images at (B) low pressure versus (C) high pressure. Images were acquired using a 3 MHz burst from a linear array (ATL L7-4) paired with a custom 1 mm × 15 mm bifurcating optical fiber bundle used to deliver laser pulses (see in panel D). The timing of the laser shot relative to the ultrasound acquisition was controlled using a programmable ultrasound system. Color images were normalized to the maximum signal in panel C and superimposed on gray scale ultrasound (US) images. The four samples from left to right are cellulose, PPy particles in water (8.1 nM), and PFP PPy emulsion contrast agent (0.65 pM), and the tube containing DI water. Cellulose provided the greatest US scattering within the tube (gray scale). Although a PA signal was produced by both the PPy particles as well as the PPy coated emulsions, only the PPy coated emulsions produced an SPA signal. Conventional US and PA imaging provides a linear signal that scales with transmitted signal intensity and absorbed energy density, respectively, which is removed from the SPA images (seen comparing panels A and B). For PPy emulsions, when the combined energy from the laser and US exceeds the cavitation threshold, the contrast agent vaporizes to produce a non-linear signal. The non-linear SPA contrast enhancement from the PPy coated PFP emulsions were compared against PA contrast imaging of PPy particles (no PFC core) (see panel E). PA imaging contrast enhancement has no dependence on transmitted acoustic pressure ($R^2 = 0.0009$), while SPA imaging shows a near linear increase in contrast enhancement with increasing pressure ($R^2 = 0.94$). The low contrast obtained from the SPA contrast agent relative to the PA agent at pressures under 0.4 MPa is due to the much lower concentration of SPA agents than PA agents. The additional signal seen in some of the ultrasound images as well as the SPA contrast image (panel D) is from an internal acoustic reflection from the tube.

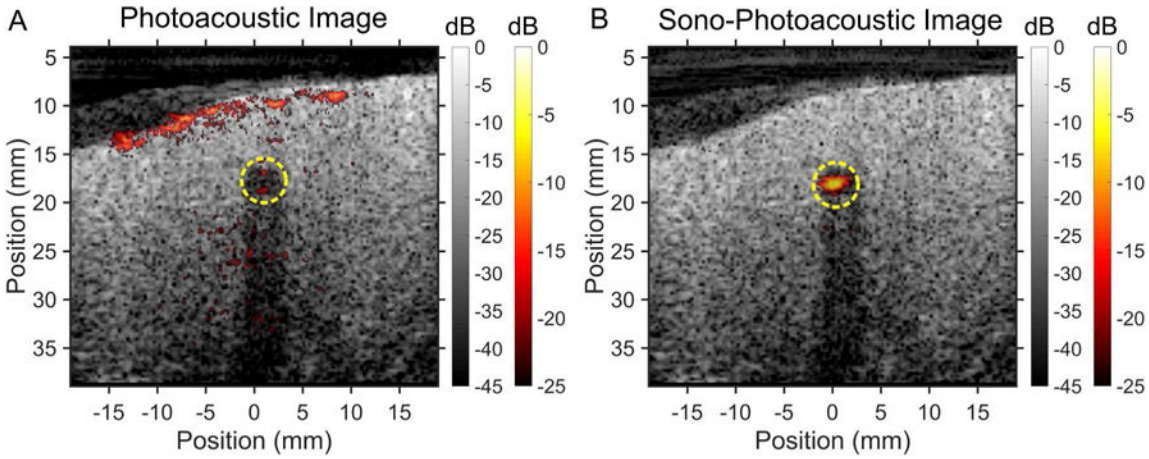

Figure 5.

Sequence of images taken using (A) PA imaging of a PA agent versus (B) SPA imaging of PPy coated PFP as the contrast agent in chicken breast tissue at room temperature (25°C). Images were acquired using a surface fluence of 45 mJ/cm^2 at λ = 1064 nm and an MI of 0.67 (1.16 MPa). The contrast agents were contained within a 4 mm diameter thin walled plastic tube (yellow dashed line) inserted into the tissue. The tube created an acoustic shadow, seen in the ultrasound images, due to acoustic reflections from the tube wall. Localizing the PA agent is made more difficult due to the PA contrast generated by the tissue itself. In addition to having greater contrast enhancement from the SPA agent during SPA imaging, the PA contrast produced from the tissue is suppressed due to linear PA signal subtraction in the SPA sequence.